

# RSC Advances



This is an *Accepted Manuscript*, which has been through the Royal Society of Chemistry peer review process and has been accepted for publication.

*Accepted Manuscripts* are published online shortly after acceptance, before technical editing, formatting and proof reading. Using this free service, authors can make their results available to the community, in citable form, before we publish the edited article. This *Accepted Manuscript* will be replaced by the edited, formatted and paginated article as soon as this is available.

You can find more information about *Accepted Manuscripts* in the [Information for Authors](#).

Please note that technical editing may introduce minor changes to the text and/or graphics, which may alter content. The journal's standard [Terms & Conditions](#) and the [Ethical guidelines](#) still apply. In no event shall the Royal Society of Chemistry be held responsible for any errors or omissions in this *Accepted Manuscript* or any consequences arising from the use of any information it contains.



## Improved power density of an enzymatic biofuel cell with fibrous supports of high curvature

A. S. Campbell,<sup>a</sup> M. V. Jose,<sup>b</sup> S. Marx,<sup>b,†</sup> S. Cornelius,<sup>b</sup> R. R. Koepsel,<sup>c,d</sup> M. F. Islam<sup>\*e</sup> and A. J. Russell<sup>\*,a,c,d,f</sup>

Received 00th January 20xx,  
Accepted 00th January 20xx

DOI: 10.1039/x0xx00000x

www.rsc.org/

Enzyme immobilization onto gold- or carbon nanotube-based nanomaterials has driven recent advances in the development of enzymatic biofuel cells (EBFCs). Enzyme-gold and enzyme-carbon nanotube interfaces are conducive to achieving efficient electron transfer between the enzyme active site and an electrode along with high enzyme loadings. Herein, we investigate the performance dependence of EBFCs on the surface curvature, specific surface area (SSA) and pore size of underlying enzyme supports. One of the supports was gold/multi-wall carbon nanotube (MWCNT) fiber paddle that were formed by depositing gold nanoparticles and MWCNTs onto electrospun polyacrylonitrile fibers with a diameter of 1  $\mu\text{m}$  and a SSA of 3.6  $\text{m}^2 \text{g}^{-1}$  with micrometer sized pores. The other support was graphene-coated single-wall carbon nanotube (SWCNT) gels, which had 1 nm thick struts, 686  $\text{m}^2 \text{g}^{-1}$  SSA, and pores of diameter  $\leq 15$  nm. Glucose oxidase (GOX) and bilirubin oxidase (BOD) were immobilized onto each material to form enzymatically active anodes and cathodes, respectively. EBFCs constructed using gold/MWCNT fiber paddle electrodes yielded power densities of 0.4  $\mu\text{W cm}^{-2}$  with an open circuit voltage of 0.22 V and GOX loadings of  $2.0 \times 10^{-10} \text{ mol cm}^{-2}$ . In comparison, EBFCs utilizing graphene-coated SWCNT gel electrodes had 10-fold lower GOX loadings ( $1.0 \times 10^{-11} \text{ mol cm}^{-2}$ ), but still produced 10-fold greater power densities ( $\approx 3.6 \mu\text{W cm}^{-2}$ ) and an open circuit voltage of 0.22 V. We postulate that a greater fraction of GOX supported on graphene-coated SWCNTs that had high curvature retained their biochemical functionality. Further, this study provides a design principle for improving enzymatic power generation.

### Introduction

Immobilized enzymes are used in a wide range of applications.<sup>1,2</sup> The conjugation of enzymes onto or within support materials serves to impart biological function to non-biological materials while providing enhanced enzyme stability and a means of retaining enzymatic activity at a surface.<sup>3-6</sup> Enzyme-based biofuel cells (EBFCs) use immobilized enzymes

to generate electrical power from renewable fuels.<sup>7,8</sup> Such systems have been reported to generate power densities of up to 2  $\text{mW cm}^{-2}$  from sugars such as glucose and fructose, thereby enabling the continuous powering of some implantable devices.<sup>9-14</sup> For EBFCs to function effectively, the working enzymes must be immobilized at or near an electrode surface so that electron transfer between the enzyme active site and the electrode structure continues during operation. The interactions at the enzyme-support interface influence these properties and thus the overall performance, making the choice of support material crucial.<sup>1,15,16</sup>

The operation of EBFCs is based on the oxidation of a fuel at the anode and the reduction of a final electron acceptor (generally molecular oxygen) at the cathode. The capability of these devices to operate at physiological conditions and the biocompatibility of reactants and products make EBFCs ideally suited for operation *in vivo*.<sup>13</sup> During operation, electrons are transferred between the enzyme active site and the electrode surface either directly (direct electron transfer (DET)) or through an intermediate redox molecule (mediated electron transfer (MET)). The achievable power density of a given EBFC is a function of both the efficiency of electron transfer, the degree of enzyme loading onto the electrode surface and the retained enzyme kinetics.<sup>17,18</sup> In designing an EBFC support material, three key parameters for consideration are support curvature, pore size and specific surface area (SSA). A porous

<sup>a</sup> Department of Biomedical Engineering, Carnegie Mellon University, 5000 Forbes Avenue, Pittsburgh, Pennsylvania 15213, United States.

<sup>b</sup> McGowan Institute for Regenerative Medicine, University of Pittsburgh, 450 Technology Drive, Pittsburgh, Pennsylvania 15219, United States.

<sup>c</sup> Disruptive Health technology Institute, Carnegie Mellon University, 5000 Forbes Avenue, Pittsburgh, Pennsylvania 15213, United States.

<sup>d</sup> The Institute for Complex Engineered Systems, Carnegie Mellon University, 5000 Forbes Avenue, Pittsburgh, Pennsylvania 15213, United States.

<sup>e</sup> Department of Materials Science & Engineering, Carnegie Mellon University, 5000 Forbes Avenue, Pittsburgh, Pennsylvania 15213, United States. Email: mohammad@cmu.edu

<sup>f</sup> Department of Biological Sciences, Carnegie Mellon University, 5000 Forbes Avenue, Pittsburgh, Pennsylvania 15213, United States. Email: alanrussell@cmu.edu

<sup>†</sup> Current address: Department of Physical Chemistry, Israel Institute for Biological Research, Ness Ziona, 74100 Israel.

Electronic Supplementary Information (ESI) available: Electrode material surface area analysis; cyclic voltammetry of electrode materials without enzyme functionalization; amperometric performance of electrode systems; cyclic voltammetry of oxygen reduction at electrode materials without enzyme functionalization; biofuel cell performance of electrode materials without enzyme functionalization. See DOI: 10.1039/x0xx00000x

material with high SSA provides ample surface area for enzyme adsorption, which can lead to high enzyme loadings. However, without appropriate pore sizes, much of the material may not be accessible to the target enzyme, effectively reducing the available surface area. Further, studies have shown a direct influence of support curvature on retained activity of immobilized enzyme.<sup>2,15,16</sup> This impact has been attributed to increased nonspecific interactions between the enzyme and surfaces with lower rates of curvature (i.e. larger diameter) as well as between adjacent enzymes leading to increased protein denaturation upon adsorption.<sup>5,16</sup> Evaluating the impact of each of these design parameters is crucial to the efficient design of future EBFC systems.

To optimize power, nanomaterials have become increasingly popular electrode materials due to their high available surface area and their potential to facilitate efficient electron transfer.<sup>19,20</sup> Nanomaterials have also been proven to be capable of enhancing immobilized enzyme stability while preserving enzyme function.<sup>3-6,21-30</sup> For instance, Wu *et al.* recently reported the significantly increased stability of a GOX-based biosensor against trypsin, ethylenediaminetetraacetic acid (EDTA) and long-term storage when the enzyme was incorporated into zeolitic imidazolate framework nanocrystals.<sup>21</sup> Two of the most widely used classes of nanomaterial are gold nanoparticle (AuNP)- and carbon nanotube-based surfaces. Both of these nanomaterials possess excellent electrical conductivity, high SSA and an ease of functionalization making them ideal for enzyme interaction.<sup>19</sup> For example, Cosnier *et al.* reported one of the highest performing and most versatile EBFC systems to date based on compressed pellets of multi-wall carbon nanotubes (MWCNTs) operating *via* DET<sup>9</sup> and MET<sup>10</sup>, which was further shown to successfully function within a rat model.<sup>12</sup> Shleev *et al.* have exhibited the potential of AuNP functionalized electrodes to form intricate systems capable of operating within the eye toward forming “smart” contact lenses.<sup>31,32</sup> Similarly, our group has investigated the capability of these materials to form high-performing biosensors and EBFCs. Our studies showed the capability of carbon nanotube- and AuNP-based materials to form highly porous networks, which allowed high enzyme loadings and reliable operation without the need for external mediators.<sup>33-35</sup> Despite significant research into developing efficient EBFCs, the application of EBFCs is currently limited due to challenges stemming from poor electron transfer efficiency and enzyme stability at the enzyme-nanomaterial interface.<sup>36</sup> A thorough understanding of the impact of electrode material characteristics such as surface curvature, SSA and pore size on resulting EBFC performance was the goal of the work described herein. Gold/MWCNT fiber paddle electrodes<sup>34</sup> and graphene-coated single-wall carbon nanotube (SWCNT) gel electrodes<sup>37,38</sup> were modified with electroactive enzymes and their electrochemical properties determined. Glucose oxidase (GOX) and bilirubin oxidase (BOD) were used as anodic and cathodic catalysts, respectively. Both of these model electroactive enzymes are used throughout EBFC and biosensor research and have been thoroughly characterized.<sup>39-42</sup> Gold/MWCNT fiber paddle

electrodes were fabricated *via* the electrospinning of polyacrylonitrile (PAN) fibers containing gold salt followed by reduction and deposition of AuNPs and subsequent coating with MWCNTs.<sup>34</sup> Graphene-coated SWCNT gels were formed by mixing suspensions of individually dispersed SWCNTs and slowly decreasing water content until percolation occurred, forming a network of interconnected SWCNTs that was then coated with a continuous graphene layer through the cyclization and reduction of glucose.<sup>37,38</sup> These two systems were characterized in terms of anodic and cathodic electrochemistry as well as EBFC performance. We also determined how material morphology and surface properties impacted performance of each electrode. The objectives of this study were to provide an in-depth, side-by-side comparison of two materials with varying surface curvature, SSA and pore size to aid in the efficient design of future EBFC and biosensor systems.

## Experimental

### Materials

Ultrapure milliQ grade water (resistivity of 18.2 MΩ cm) was used for all experiments. Sodium phosphate buffer (0.1 M, pH 7.0) was prepared from phosphate salts and used for the preparation of enzyme solutions and testing of electrodes. GOX Type VII from *Aspergillus niger* (100-250 units mg<sup>-1</sup>) was purchased from Sigma-Aldrich. BOD from *Myrothecium sp.* (2.7 U mg<sup>-1</sup>) was purchased from Amano Enzyme Inc. MWCNTs with average diameter of 11.5 nm and average length of 30 μm were purchased from Cheap Tubes, Inc. CoMoCAT SWCNTs (batch CG 200) with average diameter of 1 nm and average length of 1 μm were purchased from Southwest Nanotechnologies Inc. All chemicals were of analytical grade and used as received.

### Electrode fabrication

We prepared gold/MWCNT fiber paddle electrodes<sup>34</sup> and graphene-coated SWCNT gel electrodes<sup>37,38,43</sup> as previously described. To obviate the need for surfactant, we performed the electrophoretic deposition of MWCNTs used in the fabrication of gold/MWCNT fiber paddle electrodes with 0.02 mg mL<sup>-1</sup> MWCNTs in 33% ethanol.<sup>34</sup> For testing, we formed graphene-coated SWCNT gel electrodes in 2 mm thick rectangular molds and cut ≈ 0.5 cm<sup>2</sup> sections.

To form enzyme-modified anodes and cathodes, we incubated individual electrodes in 1 mg mL<sup>-1</sup> enzyme solution (GOX or BOD in sodium phosphate buffer (0.1 M, pH 7.0)) for 4 h at 4°C to allow enzyme attachment *via* physical adsorption. Using a bench-top vacuum pump, we applied a weak pulsed vacuum for several minutes prior to incubation of graphene-coated SWCNT gels to enhance enzyme internalization. Then, we briefly washed each electrode to remove loosely bound enzyme prior to individual electrochemical examination or EBFC testing.

### Microstructural characterization

SSA of graphene-coated SWCNT gels was measured through nitrogen adsorption and desorption at 77 K using a Gemini VII 2390 surface area analyzer (Micromeritics) using the Brunauer, Emmett and Teller (BET) theory.<sup>44</sup> Pore volume and pore size distribution were calculated from the measured desorption isotherms using the density functional theory (DFT) calculation scheme.<sup>45</sup> Scanning electron microscope (SEM) images were taken using a FEI/Aspex Explorer and FEI Quanta 600 scanning electron microscope for gold/MWCNT fiber paddle and graphene-coated SWCNT gel, respectively. Transmission electron microscope (TEM) images were collected using a FEI Titan 83 TEM.

### Electrode characterization

Total GOX loadings were determined using a standard bicinchoninic acid (BCA) assay kit (ThermoFisher Scientific). GOX-functionalized electrodes were incubated at room temperature with shaking at 100 rpm in 1 wt% sodium dodecylbenzenesulfonate (NaDDBS) for 4 h and supernatant tested for protein concentration. All electrochemical measurements were performed using a conventional three-electrode electrochemical cell utilizing a KCl saturated Ag/AgCl electrode and a 0.5 mm diameter platinum wire electrode and reference and counter electrodes, respectively. Gold/MWCNT fiber paddle electrochemically active surface area was measured through the electrochemical oxidation/reduction of ferrocenecarboxylic (FeCOOH) acid at the electrode surface *via* cyclic voltammetry (CV).<sup>35</sup> EBFC performance characteristics were evaluated in 200 mL of air saturated sodium phosphate buffer (0.1 M, pH 7.0) containing 0.1 M glucose under stirring and using a Fluke 287 True RMS multimeter with an IET Labs RS-200 resistance decade box that was used to manually vary circuit resistance.

## Results and Discussion

### Material characterization

The performance characteristics of enzyme-nanomaterial conjugates greatly depend on the surface properties of the nanomaterial.<sup>15,16</sup> Enzyme loading and substrate accessibility are a function of available surface area and porosity while specific enzyme activity and stability depend on enzyme conformation at the nanomaterial surface, which can be impacted by support surface curvature, enzyme orientation and binding affinity.<sup>19,46</sup> All of these interactions coupled with the electron transfer characteristics of the system are the target design parameters of enzyme-based bioelectronics. Many studies have shown the impact of material characteristics on enzyme biochemical activity and stability, but the effect of these material properties on enzyme electrochemical activity has not been adequately described.<sup>2,15,16</sup> Toward this goal we fabricated two differing electrode systems based on commonly used classes of nanomaterials to determine their capabilities as electroactive enzyme supports and to compare their varying performance characteristics as a function of material properties. The chosen

electrode materials were gold/MWCNT fiber paddles and graphene-coated SWCNT gels, which possessed extremely different surface curvature, pore sizes and SSA. The surface curvature of materials such as carbon nanotubes and electrospun fibers are determined by diameter, with larger diameter materials possessing a lower degree of curvature.<sup>5,15,16</sup>

We found both electrode materials consisted of interconnected porous networks of individual polymer fibers or SWCNTs (Fig. 1). SEM images of gold/MWCNT fiber paddles showed  $\approx 1 \mu\text{m}$  diameter PAN fibers coated with 0.5 – 0.7  $\mu\text{m}$  AuNPs and with 11.5 nm diameter MWCNTs (Fig. 1a-c). Pore sizes between adjacent fibers were on the order of several micrometers, which allowed unhindered access to both substrate and adsorbing enzyme.<sup>47</sup> Imaging of graphene-coated SWCNT gels revealed a percolating network of 1 nm diameter SWCNTs (Fig. 1d) coated with multiple layers of graphene (Fig. 1e). This structure was consistent with previous reports of similar materials.<sup>37,38</sup> The SSA of the gold/MWCNT fiber paddles was too low to be reliably measured by a BET system. Hence, we probed the electrochemically active surface area (ECSA) of the gold/MWCNT fiber paddles through the oxidation and reduction of the small redox molecule FeCOOH *via* CV (Fig. S1a and b).<sup>35</sup> At high scan rates, the anodic and cathodic peak currents increased linearly with scan rate, which indicated a surface-limited system.<sup>48</sup> The slopes of these curves were used to calculate the FeCOOH loading at the electrode surface, which yielded a calculated ECSA of  $3.6 \text{ m}^2 \text{ g}^{-1}$  that qualitatively reflected the SSA of the paddles.<sup>48</sup> The ECSA of a material depends on the conducting nature of the electrode being studied and is thus a measure of surface area available for interaction with redox molecules.<sup>49</sup> In this study, the ECSA is comparable to the SSA of the material as only the surface area capable of electron transfer with redox molecules would yield electrochemically active immobilized enzyme or substrate reduction/oxidation. For simplicity and comparison with graphene-coated SWCNT gels, we refer to the ECSA of the gold/MWCNT fiber paddles as SSA. We examined the SSA of

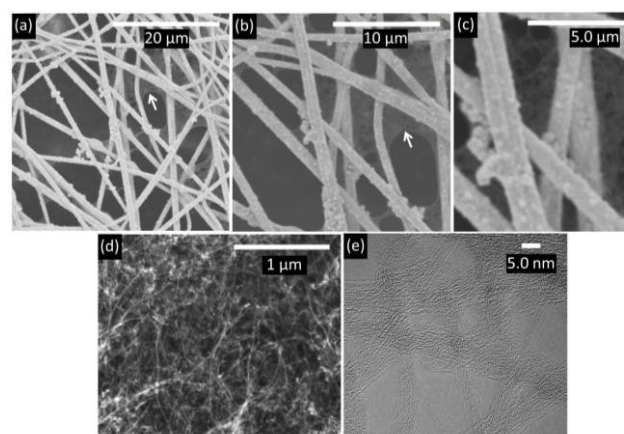


**Fig 1.** Morphological examination of electrode materials. (a-c) SEM images of gold/MWCNT fiber at varying magnifications. White arrows indicate formation of MWCNT interconnection between neighboring fibers. (d) SEM and (e) TEM images of graphene-coated SWCNT gel.

the graphene-coated SWCNT gels using BET analysis of nitrogen adsorption and desorption and modeled pore distribution using the DFT calculation scheme (Fig. S1c and d). These gels possessed a SSA of  $686 \text{ m}^2 \text{ g}^{-1}$  with the majority of the total pore volume made up of pores less than 15 nm in radius. Some of the pores were too small to allow unhindered internalization of enzymes such as GOX ( $8 \times 7 \times 8 \text{ nm}$ ) throughout the gel structure.<sup>47</sup> Both materials were further modified *via* physical adsorption of GOX and BOD and electrochemically characterized.

### Anodic system comparison

The anodic enzyme GOX catalyzes the two-electron oxidation of glucose to gluconolactone and the subsequent reduction of molecular oxygen to hydrogen peroxide. EBFC anodes utilize the oxidation half of this reaction to generate electrical current through the transfer of electrons to an electrode surface by DET or MET instead of to oxygen. Alternatively, oxidation of generated hydrogen peroxide can occur at the electrode surface effectively using molecular oxygen as a natural electron mediator.<sup>50,51</sup>

We electrochemically characterized GOX-modified anodes formed from each of the two electrode materials. CV traces of GOX-modified anodes of both materials showed obvious oxidation and reduction peaks with formal potentials of  $-0.43 \text{ V}$  versus Ag/AgCl. This formal potential was indicative of quasi-reversible oxidation/reduction of the flavin adenine dinucleotide (FAD)-based active site of GOX (Fig. 2). The identical formal potential of the two systems suggested a

similar conformation of electrochemically active GOX at the enzyme-nanomaterial interface in both systems. Graphene-coated SWCNT gel anodes exhibited a significantly higher capacitive current response than our gold/MWCNT fiber paddle anodes. We believe this property reflected the larger SSA of the graphene-coated SWCNT gel as opposed to our gold/MWCNT fiber paddles.<sup>52</sup> To better exhibit the faradaic peaks of GOX at graphene-coated SWCNT gels, we additionally performed the CV analysis at a lower scan rate of  $5 \text{ mV s}^{-1}$ , which yielded identical results (Fig. S2). Upon the addition of glucose to either GOX-modified anode, we observed no appreciable shift in current response. This result demonstrated that no current generation was being driven by DET and suggested that current was produced *via* hydrogen peroxide oxidation using oxygen as a natural electron mediator. No faradaic peaks or shifts in current were observed in trials with materials lacking GOX modification (Fig. 2 and Fig. S3).

By performing CV scans at varying scan rates, we were able to determine the loading of FAD at the anodic material surface and the heterogeneous electron transfer rate constant ( $k_s$ ). We calculated the loadings of FAD using the dependence of anodic and cathodic peak currents with increasing scan rate. The linearity of this plot indicated that the efficiencies of both systems were limited by the rate of electron transfer to the electrode surface rather than diffusion.<sup>33,48</sup> Gold/MWCNT fiber paddle anodes had an electrochemical loading of  $3.92 \times 10^{-10} \text{ mol FAD cm}^{-2}$  whereas graphene-coated SWCNT gel anodes had an electrochemical loading of  $1.99 \times 10^{-11} \text{ mol FAD cm}^{-2}$  (where the area was the cross-sectional area of the electrode). We examined the accuracy of these values in representing the total GOX loading by removing adsorbed enzymes from GOX-functionalized electrodes using the surfactant NaDDBS and testing the resulting supernatants *via* standard BCA assay. The resulting total GOX loadings were  $2.60 \times 10^{-10} \text{ mol GOX cm}^{-2}$  and  $1.57 \times 10^{-11} \text{ mol GOX cm}^{-2}$  for gold/MWCNT fiber paddle anodes and graphene-coated SWCNT gel anodes, respectively. These values were slightly higher than the apparent loadings determined electrochemically assuming two FAD molecules corresponded to one GOX molecule. The increased total loading compared to the electrochemically determined loading is likely due to one or both FAD sites in some adsorbed GOX molecules not being electrochemically connected to the electrode surface, which is consistent with similar materials.<sup>53</sup> These loading results suggested extensive GOX coverage throughout the gold/MWCNT fiber paddles, but limited internalization into the graphene-coated SWCNT gels, meaning that GOX was likely only adsorbed at the outer gel surface. We further calculated the  $k_s$  for each system using the dependence of anodic and cathodic peak potentials on the logarithm of scan rate.<sup>33,54,55</sup> We found the  $k_s$  values to be  $0.95 \pm 0.01 \text{ s}^{-1}$  and  $0.98 \pm 0.07 \text{ s}^{-1}$  for gold/MWCNT fiber paddle anodes and graphene-coated SWCNT gel anodes, respectively. Electron transfer resistances between adsorbed FAD and the electrode surface were clearly similar in both systems, which further suggested similar conformation of electrochemically active GOX at the electrode surfaces.

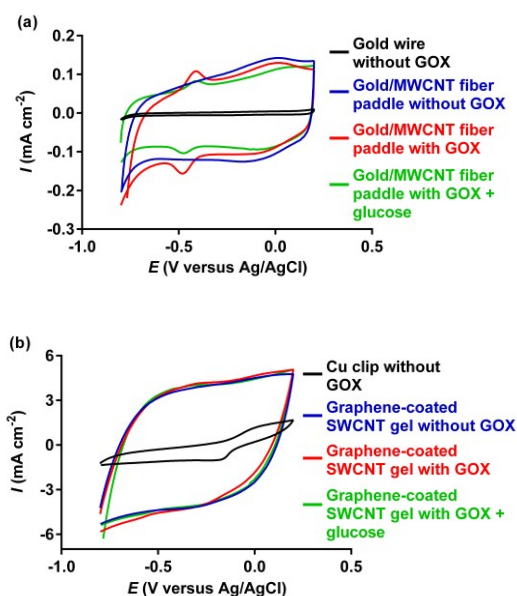


**Fig 2.** Electrochemical performance of anodic systems. (a) CV traces of gold wire, gold/MWCNT fiber paddle anode, GOX-modified gold/MWCNT fiber paddle anode and GOX-modified gold/MWCNT fiber paddle anode in 0.1 M glucose. (b) CV traces of copper clip, graphene-coated SWCNT gel anode, GOX-modified graphene-coated SWCNT gel anode and GOX-modified graphene-coated SWCNT gel anode in 0.1 M glucose. Experiments performed in Ar saturated sodium phosphate buffer (0.1 M, pH 7.0) at  $50 \text{ mV s}^{-1}$  scan rate.

The appearance of faradaic peaks in CV traces of GOX-modified materials confirmed the presence of electrochemically active FAD at the electrode surface, but these data alone did not definitively prove that GOX was biochemically active (Fig. 2).<sup>51</sup> To examine if biochemically active GOX was successfully adsorbed onto the electrode materials, we monitored the current output of each GOX-modified anode upon the successive addition of glucose (Fig. S4). When the potential of the each anode was held at 0.8 V versus Ag/AgCl in an oxygen saturated solution, an obvious increase in anodic current was observed (Fig. S4). This response corresponded to the electrochemical oxidation of hydrogen peroxide produced by GOX, which confirmed the presence of biochemically active GOX turning over glucose in both systems under study.<sup>34,56</sup>

Examination of the increasing current density upon glucose addition allowed the calculation of maximum current density ( $J_{max}$ ) and apparent Michaelis-Menten constant ( $K_M$ ) for both systems (Fig. S4). The GOX-functionalized gold/MWCNT fiber paddle anodes yielded a  $J_{max}$  of  $0.23 \pm 0.01$  mA cm<sup>-2</sup> and an apparent  $K_M$  of  $18.8 \pm 2.6$  mM glucose, whereas the GOX-functionalized graphene-coated SWCNT gel anodes achieved a  $J_{max}$  of  $0.57 \pm 0.03$  mA cm<sup>-2</sup> with an apparent  $K_M$  of  $33.8 \pm 4.8$  mM glucose. Coupled with the calculated total GOX loadings, these  $J_{max}$  values become  $8.85 \times 10^8$  mA mol<sup>-1</sup> of GOX and  $3.63 \times 10^{10}$  mA mol<sup>-1</sup> of GOX for the gold/MWCNT fiber paddle anodes and the graphene-coated SWCNT gel anodes, respectively. The higher current generation rate per mol of GOX immobilized onto the graphene-coated SWCNT gel electrode suggested much greater biochemical activity at the electrode surface. This finding was consistent with reports stating that enzymes adsorbed onto curved nanomaterials retain more activity on supports with smaller diameters.<sup>5,16</sup> Interestingly, GOX adsorbed onto the graphene-coated SWCNT gel electrode also exhibited an increased apparent  $K_M$ , which was indicative of interference with substrate binding by the smaller diameter SWCNTs. The detection of hydrogen peroxide oxidation showed the capability of both material systems to perform as functioning enzyme-based electrodes. However, when the working electrode potential was held at the observed FAD formal potential (-0.43 V versus Ag/AgCl) in Ar saturated solution, no sustained current response was observed for either anode material (Fig. S4) (small peaks observed resulted from mixing effects). The absence of a current response upon glucose injection under these conditions confirmed the inability of either electrode material to collect electrons from the GOX active site *via* DET. In contrast, in a previous study, we showed the capability of a similar anodic material made up of a graphene/SWCNT cogel to achieve DET with GOX.<sup>33</sup> The larger pore sizes of the cogel material aided in greater GOX internalization compared to the graphene-coated SWCNT gels, suggesting that GOX must be entirely surrounded by a nanoscale conducting material, such as SWCNTs, in order to exhibit DET, which is consistent with previous reports.<sup>57-59</sup>

We further characterized the GOX-modified anodes in terms of open circuit voltage (OCV) to analyze the extent of

overpotentials that limited the rate of electron transfer between GOX and each electrode material (Fig. 3). Analysis of the GOX-modified gold/MWCNT fiber paddle anodes in an Ar-saturated solution with 0.1 M glucose resulted in an OCV of 0.18 V versus Ag/AgCl, which was significantly higher than the thermodynamically determined value of -0.36 V versus Ag/AgCl.<sup>60</sup> We hypothesize that at least some of this effect was caused by oxygen reduction at the gold/MWCNT fiber paddle anode surface at voltages of  $\sim 0$  V versus Ag/AgCl and lower (Fig. S5a). Since OCV is a measure of the voltage at which no current is observed, at voltages below this threshold, oxygen that remained or diffused into the Ar saturated solution was likely reduced to water and generated cathodic current. GOX-modified gold/MWCNT fiber paddle anodes yielded small cathodic current due to the local depletion of oxygen *via* GOX reaction. However, reduction of oxygen still occurred (Fig. S5b). Examination of the GOX-modified graphene-coated SWCNT gel anodes under the same conditions resulted in an OCV of -0.15 V versus Ag/AgCl (Fig. 3b). The observed overpotentials could also have been caused by partial GOX denaturation or steric hindrance of its active site upon immobilization yielding reduced activity and electron transfer resistances between the buried active site of GOX and the electrode surface, which contributed to the deterrence of electron transfer.<sup>40</sup> Larger overpotentials at the gold/MWCNT fiber paddle electrode were consistent with increased GOX deformation and hence lower biochemical activity at the larger diameter gold/MWCNT fibers.

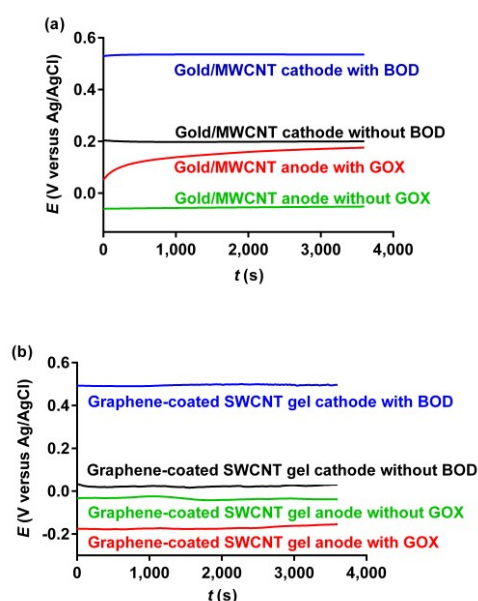
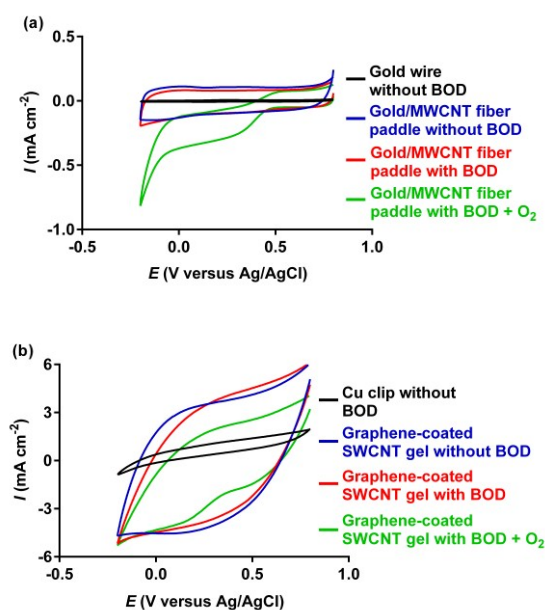


Fig. 3. Open circuit voltage analysis of electrode materials. (a) Open circuit voltage measurements of gold/MWCNT fiber paddle-based anode with and without GOX, and cathode with and without BOD. (b) Open circuit voltage measurements of graphene-coated SWCNT gel-based anode with and without GOX, and cathode with and without BOD. Experiments performed in sodium phosphate buffer (0.1 M, pH 7.0) containing substrate. Anodic measurements carried out in Ar saturated solution with 0.1 M glucose and cathodic measurements in oxygen saturated solution.

### Cathodic system comparison

The cathodic multicopper oxidase BOD catalyzes the four-electron reduction of oxygen to water at its T2/T3 copper-containing active site upon accepting electrons at its T1 copper-containing active site.<sup>42</sup> To determine the presence of overpotentials in the cathodic systems, we analyzed BOD-modified gold/MWCNT fiber paddle cathodes and BOD-modified graphene-coated SWCNT gel cathodes using OCV (Fig. 3). The enzyme-modified cathodes yielded OCVs of 0.53 V versus Ag/AgCl and 0.50 V versus Ag/AgCl for gold/MWCNT fiber paddle cathodes and graphene-coated SWCNT gel cathodes, respectively (Fig. 3). These values were consistent with the thermodynamically determined value of the T1 copper site of BOD.<sup>61</sup> The increase in OCV compared to non-modified control showed the presence of successfully adsorbed BOD with no appreciable overpotentials. To further examine cathodic characteristics, we performed CV scans of each cathode material before and after BOD modification (Fig. 4). No faradaic peaks were observed for either material system, which is consistent with previous studies.<sup>33,62</sup> BOD-modified gold/MWCNT fiber paddle cathodes showed obvious oxygen reduction at onset potentials of 0.45 V versus Ag/AgCl and 0 V versus Ag/AgCl (Fig. 4a). Non-modified gold/MWCNT fiber paddle cathodes only exhibited oxygen reduction beginning at 0 V versus Ag/AgCl consistent with anodic measurements, which confirmed BOD adsorption and DET (Fig. S6a). Similarly, BOD-modified graphene-coated SWCNT gel



**Fig 4.** Electrochemical performance of cathodic systems. (a) CV traces of gold wire, gold/MWCNT fiber paddle cathode, BOD-modified gold/MWCNT fiber paddle cathode in Ar saturated solution and BOD-modified gold/MWCNT fiber paddle cathode in oxygen saturated solution. (b) CV traces of copper clip, graphene-coated SWCNT gel cathode, BOD-modified graphene-coated SWCNT gel cathode in Ar saturated solution and BOD-modified SWCNT gel cathode in oxygen saturated solution. Experiments performed in sodium phosphate buffer (0.1 M, pH 7.0) at 50 mV s<sup>-1</sup> scan rate.

cathodes exhibited oxygen reduction at an onset potential of 0.4 V versus Ag/AgCl whereas no oxygen reduction was observed in non-modified trials, which confirmed DET with physically adsorbed BOD (Fig. 4b and Fig. S6b). The capability of both cathodic materials to achieve DET with adsorbed BOD was additionally confirmed *via* amperometry (Fig. S7). We observed a rapid increase in cathodic current upon oxygen bubbling into Ar saturated solution for both gold/MWCNT fiber paddle cathodes and graphene-coated SWCNT gel electrodes. Larger current density at the graphene-coated SWCNT gel electrode suggested increased loading and/or biochemical activity of BOD. Combined, these results highlighted the capability of BOD to achieve efficient DET with AuNP- and carbon nanotube-based materials whereas this functionality was not observed for surface adsorbed GOX. Efficient electron transfer from the BOD active site to electrodes with these types of materials was consistent with previous findings.<sup>33,63-65</sup>

### EBFC comparison

We separately examined symmetric EBFCs consisting of a single GOX-modified anode and a single BOD-modified cathode using either gold/MWCNT fiber paddle electrodes or graphene-coated SWCNT electrodes. All trials consisted of the manual variation of circuit resistance and the monitoring of resulting cell voltages in air saturated sodium phosphate buffer (0.1 M, pH 7.0) containing glucose (0.1 M). Gold/MWCNT fiber paddle electrode-based systems yielded a maximum power density of  $0.42 \pm 0.06 \mu\text{W cm}^{-2}$  and full-cell OCV of  $0.22 \pm 0.02$  V (Fig. 5a). Graphene-coated SWCNT gel-based systems generated  $\sim 10$  times larger maximum power density of  $3.56 \pm 1.09 \mu\text{W cm}^{-2}$  but identical full-cell OCV of  $0.22 \pm 0.03$  V (Fig. 5b). Recall that the graphene-coated SWCNT gel electrodes had  $\sim 10$  times lower GOX loading. The identical OCV values confirmed similar electron transfer limitations in both systems where the increased power density of the graphene-coated SWCNT gel-based system was consistent with a higher degree of GOX biochemical activity at the anode. Further, when the EBFC systems were examined without enzyme-modification, we observed negligible power density, which confirmed GOX and BOD were solely responsible for power generation (Fig. S8). Individual characterization of the anodic and cathodic components of each system showed EBFCs made up of either material to be limited at the anode as electron transfer was not hindered by cathodic overpotentials and efficient DET with BOD was observed.

For comparison, we calculated the theoretical power density of each system based on the electrochemically determined GOX loading and operating voltage that correlated to the maximum power density. Assuming GOX operation at the previously determined native  $k_{cat}$ , experimental maximum power densities corresponded to 0.03% and 4.28% of theoretical values for gold/MWCNT fiber paddle- and graphene-coated SWCNT gel-based systems, respectively.<sup>33</sup> This result showed that despite allowing a twenty-fold higher GOX loading due to unhindered internalization by larger pore sizes, the gold/MWCNT fiber paddle-based system yielded a

~10 fold lower maximum power density than the graphene-coated SWCNT gel-based system. Enzymes immobilized onto curved nanomaterials have been shown to lose a greater percentage of enzymatic activity when adsorbed onto supports with lower degrees of curvature (i.e., larger diameter). This has been attributed to increased interaction between hydrophobic portions of the enzyme surface and the hydrophobic nanomaterial surface leading to a greater degree of enzyme deformation upon adsorption.<sup>16</sup> Thus, it was possible that the larger diameter PAN fibers coated with AuNPs and MWCNTs in the gold/MWCNT fiber paddle system caused relatively greater GOX denaturation upon adsorption compared to the graphene-coated SWCNT gel system. The forty-fold greater current generation rate per mol of GOX observed at the graphene-coated SWCNT gel anode was consistent with higher GOX specific activity at the electrode material of higher curvature. These results highlighted the importance of not only targeting high working enzyme loadings, but also providing maximum retained activity and charge collection capability.

The two EBFC systems described in this study allowed us to delve into the interactions of electroactive enzymes with commonly used electrode materials. We recently described an EBFC that had significantly higher power density that is included in Fig. 5c-d.<sup>33</sup> The increased power density of this graphene/SWCNT cogel-based EBFC was driven by a GOX loading two to three orders of magnitude greater than the

systems discussed in this study, but with GOX fully internalized into a three-dimensional conducting matrix. The increased GOX loading was possible due to the high SSA of the graphene/SWCNT cogels ( $846 \text{ m}^2 \text{ g}^{-1}$ ) coupled with pore sizes that allowed unhindered access of GOX throughout the electrode material (70% of pores greater than 10 nm).<sup>33</sup> The encapsulation of GOX into the electrode structure allowed some measure of DET to be achieved, but yielded decreased current generation efficiency (0.08% relative to native GOX at the observed loading) compared with the graphene-coated SWCNT gel-based system, which possessed a comparable SSA ( $686 \text{ m}^2 \text{ g}^{-1}$ ).<sup>33</sup> This result emphasized the need for electrode materials to possess not only high SSA, but also appropriate pore sizes to maximize enzyme accessible surface area. The high anodic loading allowed this system to produce a power density within one order of magnitude of the highest performing systems reported to date.<sup>9-11,33,66</sup> Together, the data we have generated on these three EBFC designs has taught us that ample SSA for enzyme adsorption, appropriate pore size for enzyme/substrate internalization and high surface curvature for retained enzyme activity were critical elements in driving efficacy.

## Conclusions

We have thoroughly characterized and compared glucose-driven EBFCs based on two vastly differing materials. We

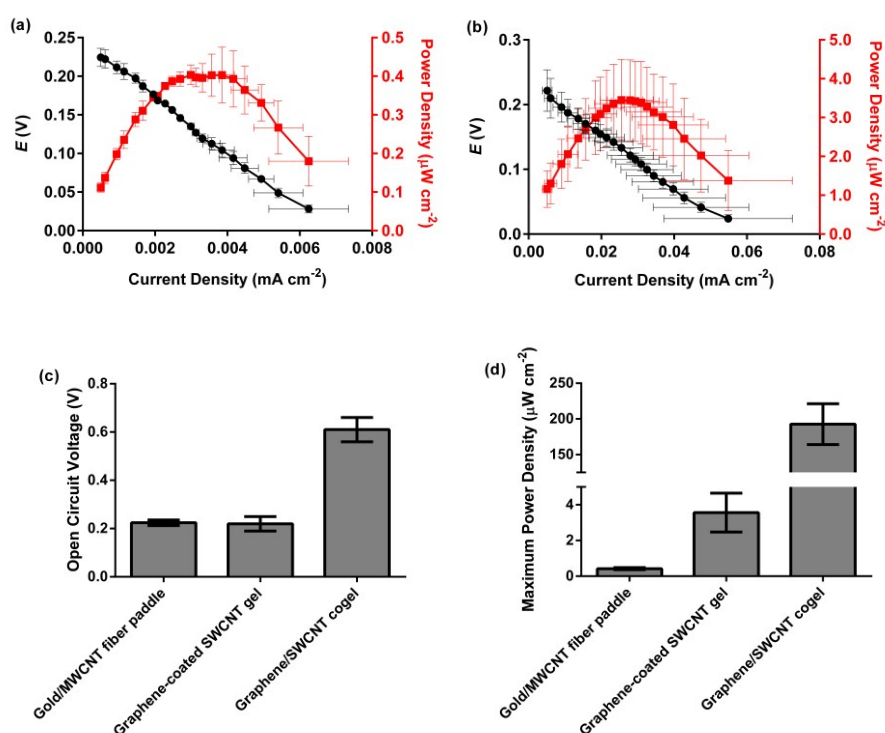


**Fig 5.** EBFC performance comparison of electrode materials. (a) Gold/MWCNT fiber paddle-based EBFC performance and cell polarization curves. (b) Graphene-coated SWCNT gel-based EBFC performance and cell polarization curves. Experiments performed in air saturated sodium phosphate buffer (0.1 M, pH 7.0) with 0.1 M glucose. (c) Open circuit voltage comparison of gold/MWCNT fiber paddle-, graphene-coated SWCNT gel- and graphene/SWCNT cogel-based EBFCs. (d) Maximum power density comparison of gold/MWCNT fiber paddle-, graphene-coated SWCNT gel- and graphene/SWCNT cogel-based EBFCs. Error bars represent standard deviation of three trials.<sup>33</sup>

showed that gold/MWCNT fiber paddle electrodes and graphene-coated SWCNT gel electrodes were capable of generating power densities of  $0.42 \pm 0.06 \mu\text{W cm}^{-2}$  and  $3.56 \pm 1.09 \mu\text{W cm}^{-2}$  with OCVs of  $0.22 \pm 0.02 \text{ V}$  and  $0.22 \pm 0.03 \text{ V}$ , respectively, upon modification with GOX and BOD. We found that electroactive enzyme performance was a function of support curvature, pore size distribution and SSA. This work highlighted the potential of both materials to operate as enzyme-modified electrodes, and also demonstrated the limitations of each with DET between GOX and electrode surfaces remaining one of the most challenging hurdles in EBFC design. Future work will be focused on improving anodic electron transfer efficiency of GOX.

## Acknowledgements

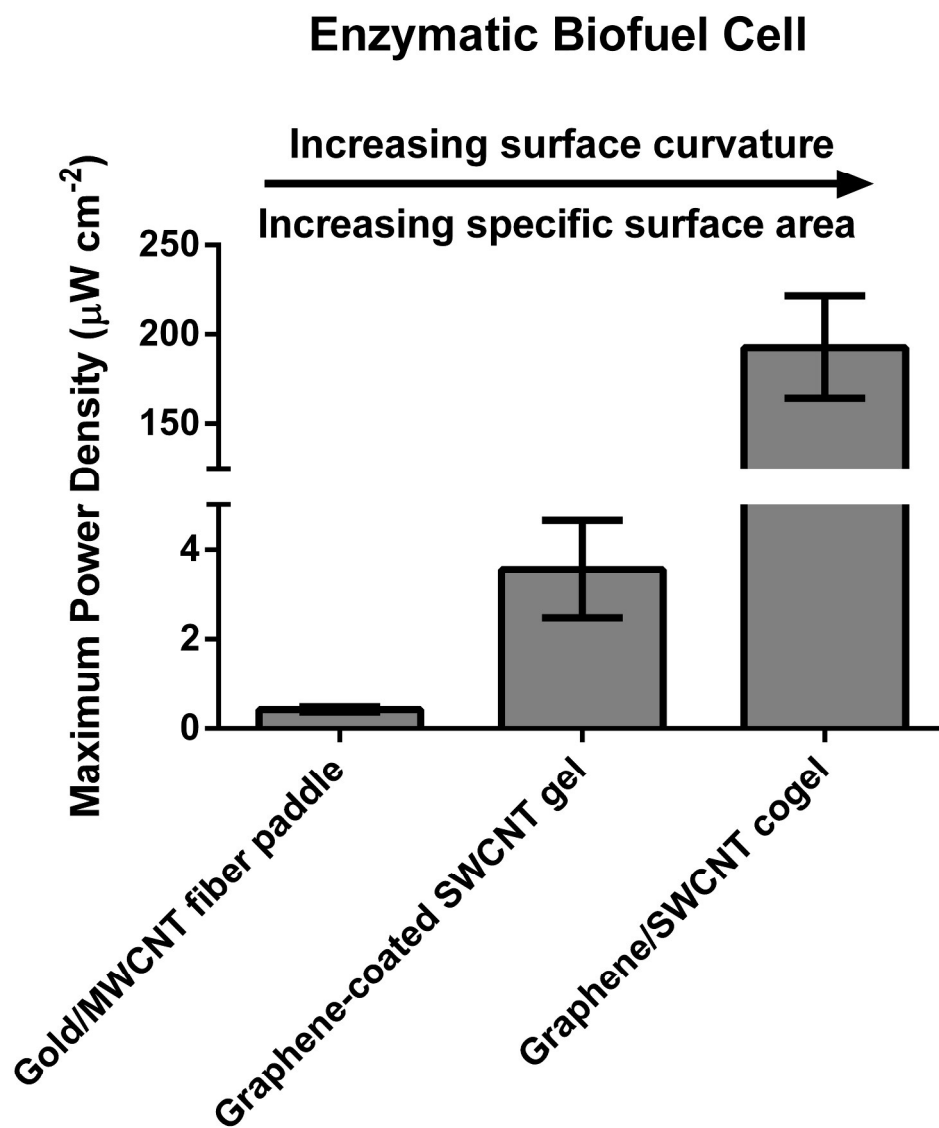
Financial support for this work was provided by Heinz Endowment through grant E0530 (AJR) and by National Science Foundation through grants CBET-1066621 (AJR) and CMMI-1335417 (MFI). We acknowledge Materials Characterization Facility of Carnegie Mellon University for TEM and SEM imaging.

## Notes and references

- S. Datta, L. R. Christena, Y. R. S. Rajaram, *Biotech*, 2013, **3**, 1-9.
- R. A. Sheldon, S. van Pelt, *Chem. Soc. Rev.*, 2013, **42**, 6223-6235.
- C. Z. Dinu, I. V. Borkar, S. S. Bale, A. S. Campbell, R. S. Kane, J. S. Dordick, *J. Mol. Catal. B: Enzym.*, 2012, **75**, 20-26.
- S. A. Ansari, Q. Husain, *Biotechnol. Adv.*, 2012, **30**, 512-523.
- P. Asuri, S. S. Karajanagi, H. C. Yang, T. J. Yim, R. S. Kane, J. S. Dordick, *Langmuir*, 2006, **22**, 5833-5836.
- A. S. Campbell, C. B. Dong, J. S. Dordick, C. Z. Dinu, *Process Biochem.*, 2013, **48**, 1355-1360.
- X. Y. Yang, G. Tian, N. Jiang, B. L. Su, *Energy Environ. Sci.*, 2012, **5**, 5540-5563.
- A. Sassolas, L. J. Blum, B. D. Leca-Bouvier, *Biotechnol. Adv.*, 2012, **30**, 489-511.
- A. Zebda, C. Gondran, A. Le Goff, M. Holzinger, P. Cinquin, S. Cosnier, *Nat. Commun.*, 2011, **2**, 370.
- B. Reuillard, A. Le Goff, C. Agnes, M. Holzinger, A. Zebda, C. Gondran, K. Elouarzaki, S. Cosnier, *Phys. Chem. Chem. Phys.*, 2013, **15**, 4892-4896.
- C. H. Kwon, S. H. Lee, Y. B. Choi, J. A. Lee, S. H. Kim, H. H. Kim, G. M. Spinks, G. G. Wallace, M. D. Lima, M. E. Kozlov, R. H. Baughman, S. J. Kim, *Nat. Commun.*, 2014, **5**, 3928.
- A. Zebda, S. Cosnier, J. P. Alcaraz, M. Holzinger, A. Le Goff, C. Gondran, F. Boucher, F. Giroud, K. Gorgy, H. Lamraoui, P. Cinquin, *Sci. Rep.*, 2013, **3**, 1516.
- S. Cosnier, A. Le Goff, M. Holzinger, *Electrochem. Commun.*, 2014, **38**, 19-23.
- K. So, S. Kawai, Y. Hamano, Y. Kitazumi, O. Shirai, M. Hibi, J. Ogawa, K. Kano, *Phys. Chem. Chem. Phys.*, 2014, **16**, 4823-4829.
- A. S. Campbell, C. B. Dong, F. K. Meng, J. Hardinger, G. Perhinschi, N. Q. Wu, C. Z. Dinu, *ACS Appl. Mater. Interfaces*, 2014, **6**, 5393-5403.
- P. Asuri, S. S. Bale, S. S. Karajanagi, R. S. Kane, *Curr. Opin. Biotechnol.*, 2006, **17**, 562-568.
- M. T. Meredith, S. D. Minteer, *Annu. Rev. Anal. Chem.*, 2012, **5**, 157-179.
- R. A. Bullen, T. C. Arnot, J. B. Lakeman, F. C. Walsh, *Biosens. Bioelectron.*, 2006, **21**, 2015-2045.
- A. de Poulpique, A. Ciaccafava, E. Lojou, *Electrochim. Acta*, 2014, **126**, 104-114.
- A. Walcarius, S. D. Minteer, J. Wang, Y. H. Lin, A. Merkoci, *J. Mater. Chem. B*, 2013, **1**, 4878-4908.
- X. Wu, J. Ge, C. Yang, M. Hou, Z. Liu, *Chem. Commun.*, 2015, **51**, 13408.
- Z. Li, Y. Zhang, Y. Su, P. Ouyang, J. Ge, Z. Liu, *Chem. Commun.*, 2014, **50**, 12465.
- J. Ge, J. Lei, R. N. Zare, *Nat. Nanotechnol.*, 2012, **7**, 428-432.
- X. Wu, C. Yang, J. Ge, Z. Liu, *Nanoscale*, 2015, **7**, 18883-18886.
- F. Lyu, Y. Zhang, R. N. Zare, J. Ge, Z. Liu, *Nano Lett.*, 2014, **14**, 5761-5765.
- X. Wu, M. Hou, J. Ge, *Catal. Sci. Technol.*, 2015, **5**, 5077-5085.
- J. Ge, C. Yang, J. Zhu, D. Lu, Z. Liu, *Top. Catal.*, 2012, **55**, 1070-1080.
- J. Ge, D. Lu, Z. Liu, Z. Liu, *Biochem. Eng. J.*, 2009, **44**, 53-59.
- L. Zhu, L. Gong, Y. Zhang, R. Wang, J. Ge, Z. Liu, R. Zare, *Chem. Asian J.*, 2013, **8**, 2358-2360.
- R. Wang, Y. Zhang, D. Lu, J. Ge, Z. Liu, R. N. Zare, *WIREs Nanomed. Nanobi.*, 2013, **5**, 320-328.
- M. Falk, V. Andoralov, Z. Blum, J. Sotres, D. B. Suyatin, T. Ruzgas, T. Arnebrant, S. Shleev, *Biosens. Bioelectron.*, 2012, **37**, 38-45.
- M. Falk, V. Andoralov, M. Silow, M. D. Toscano, S. Shleev, *Anal. Chem.*, 2013, **85**, 6342-6348.
- A. S. Campbell, Y. J. Jeong, S. M. Geier, R. R. Koepsel, A. J. Russell, M. F. Islam, *ACS Appl. Mater. Interfaces*, 2015, **7**, 4056-4065.
- M. V. Jose, S. Marx, H. Murata, R. R. Koepsel, A. J. Russell, *Carbon*, 2012, **50**, 4010-4020.
- S. Marx, M. V. Jose, J. D. Andersen, A. J. Russell, *Biosens. Bioelectron.*, 2011, **26**, 2981-2986.
- M. H. Osman, A. A. Shah, F. C. Walsh, *Biosens. Bioelectron.*, 2011, **26**, 3087-3102.
- K. H. Kim, Y. Oh, M. F. Islam, *Nat. Nanotechnol.*, 2012, **7**, 562-566.
- E. Wilson, M. F. Islam, *ACS Appl. Mater. Interfaces*, 2015, **7**, 5612-5618.
- S. B. Bankar, M. V. Bule, R. S. Singhal, L. Ananthanarayan, *Biotechnol. Adv.*, 2009, **27**, 489-501.
- G. Wohlfahrt, S. Witt, J. Hendle, D. Schomburg, H. M. Kalisz, H. J. Hecht, *Acta Crystallogr. Sect. D: Biol. Crystallogr.*, 1999, **55**, 969-977.
- N. Mano, *Appl. Microbiol. Biotechnol.*, 2012, **96**, 301-307.
- S. Brocato, C. Lau, P. Atanassov, *Electrochim. Acta*, 2012, **61**, 44-49.
- M. F. Islam, E. Rojas, D. M. Bergey, A. T. Johnson, A. G. Yodh, *Nano Lett.*, 2003, **3**, 269-273.
- S. Brunauer, P. H. Emmett, E. Teller, *J. Am. Chem. Soc.*, 1938, **60**, 309-319.
- K. H. Kim, Y. Oh, M. F. Islam, *Adv. Funct. Mater.*, 2013, **23**, 377-383.
- W. S. Liu, L. Wang, R. R. Jiang, *Top. Catal.*, 2012, **55**, 1146-1156.
- F. R. F. Fan, A. J. Bard, *Proc. Natl. Acad. Sci. U. S. A.*, 1999, **96**, 14222-14227.
- J. Wang, 2000. *Analytical Electrochemistry*, 2nd ed. John Wiley & Sons, New York.
- A. J. Bard, L. R. Faulkner, 2001. *Electrochemical Methods: Fundamentals and Applications*, 2nd ed. Wiley, New York.
- J. M. Goran, E. N. H. Phan, C. A. Favela, K. J. Stevenson, *Anal. Chem.*, 2015, **87**, 5989-5996.
- J. M. Goran, S. M. Mantilla, K. J. Stevenson, *Anal. Chem.*, 2013, **85**, 1571-1581.

- 52 M. D. Stoller, S. J. Park, Y. W. Zhu, J. H. An, R. S. Ruoff, *Nano Lett.*, 2008, **8**, 3498-3502.
- 53 B. Liang, X. Guo, L. Fang, Y. Hu, G. Yang, Q. Zhu, J. Wei, X. Ye, *Electrochem. Commun.*, 2015, **50**, 1-5.
- 54 E. Laviron, *J. Electroanal. Chem.*, 1979, **101**, 19-28.
- 55 E. Laviron, L. Roullier, *J. Electroanal. Chem.*, 1980, **115**, 65-74.
- 56 J. Wang, *Chem. Rev.*, 2008, **108**, 814-825.
- 57 M. V. A. Martins, A. R. Pereira, R. A. S. Luz, R. M. Lost, F. N. Crespitho, *Phys. Chem. Chem. Phys.*, 2014, **16**, 17426-17436.
- 58 Y. Degani, A. Heller, *J. Am. Chem. Soc.*, 1988, **110**, 2615-2620.
- 59 Y. Degani, A. Heller, *J. Phys. Chem.*, 1987, **91**, 1285-1289.
- 60 A. Heller, *Phys. Chem. Chem. Phys.*, 2004, **6**, 209-216.
- 61 A. Christenson, S. Shleev, N. Mano, A. Heller, L. Gorton, *Biochim. Biophys. Acta: Bioenerg.*, 2006, **1757**, 1634-1641.
- 62 S. Shleev, A. El Kasmi, T. Ruzgas, L. Gorton, *Electrochem. Commun.*, 2004, **6**, 934-939.
- 63 P. Ramirez, N. Mano, R. Andreu, T. Ruzgas, A. Heller, L. Gorton, S. Shleev, *Biochim. Biophys. Acta: Bioenerg.*, 2008, **1777**, 1364-1369.
- 64 K. Murata, K. Kajiyama, N. Nakamura, H. Ohno, *Energy Environ. Sci.*, 2009, **2**, 1280-1285.
- 65 W. Zheng, H. Y. Zhao, H. M. Zhou, X. X. Xu, M. H. Ding, Y. F. Zheng, *J. Solid State Electrochem.*, 2010, **14**, 249-254.
- 66 K. P. Prasad, Y. Chen, P. Chen, *ACS Appl. Mater. Interfaces*, 2014, **6**, 3387-3393.

We developed and characterized two separate enzymatic biofuel cell systems attributing improved performance to electrode support morphological characteristics.



125x151mm (600 x 600 DPI)